

Supplement of *Clim. Past*, 16, 973–1006, 2020
<https://doi.org/10.5194/cp-16-973-2020-supplement>
© Author(s) 2020. This work is distributed under
the Creative Commons Attribution 4.0 License.



Supplement of

Paleogeographic controls on the evolution of Late Cretaceous ocean circulation

Jean-Baptiste Ladant et al.

Correspondence to: Jean-Baptiste Ladant (jbladant@umich.edu)

The copyright of individual parts of the supplement might differ from the CC BY 4.0 License.

		Water transport (Sv)							
		Surface (0 - 500 m)		Intermediate (500 - 1500 m)		Deep (> 1500 m)		Total	
		-20.8 (12.9 - 33.7)		-8.8 (0.9 - 9.8)		0		-29.6 (13.8 - 43.5)	
Caribbean (>0 eastward)		-5.5 (3.1 - 8.6)	-7.4 (9.7 - 17.1)	0	0 (0.6 - 0.6)	0	4.4 (4.6 - 0.2)	-5.5 (3.1 - 8.6)	-3.0 (14.9 - 17.9)
		-6.0 (3.1 - 9.1)	-5.6 (3.1 - 8.7)	0	0	0	0	-6.0 (3.1 - 9.1)	-5.6 (3.1 - 8.7)
		-5.0 (3.3 - 8.3)	-5.7 (3.0 - 8.7)	0	0	0	0	-5.0 (3.3 - 8.3)	-5.7 (3.0 - 8.7)
		2.7 (4.8 - 2.1)		-0.6 (0.2 - 0.8)		-0.3 (0 - 0.3)		1.8 (5.0 - 3.2)	
Central Atlantic (>0 northward)		0.1 (7.6 - 7.5)	1.1 (8.1 - 7.0)	-1.3 (0.4 - 1.6)	-0.3 (0.5 - 0.8)	1.8 (2.4 - 0.6)	-3.1 (0.5 - 3.6)	0.6 (10.4 - 9.7)	-2.3 (9.1 - 11.4)
		0.3 (8.1 - 7.8)	0.2 (7.4 - 7.2)	-1.4 (0.4 - 1.8)	-0.7 (0.2 - 1.0)	1.9 (2.5 - 0.6)	1.3 (1.8 - 0.5)	0.8 (11.0 - 10.2)	0.8 (9.4 - 8.7)
		0.1 (7.8 - 7.7)	-0.7 (7.9 - 8.5)	-2.3 (0.6 - 2.9)	-2.0 (0.5 - 2.5)	2.3 (2.8 - 0.5)	-3.0 (0.6 - 3.6)	0.1 (11.2 - 11.1)	-5.7 (9.0 - 14.6)
		0.4 (0.7 - 0.4)		0.4 (0.4 - 0)		0		0.7 (1.1 - 0.4)	
Drake (>0 Pacific to Atlantic)		1.4 (3.2 - 1.8)	1.3 (3.2 - 1.9)	0	0	0	0	1.4 (3.2 - 1.8)	1.3 (3.2 - 1.9)
		1.5 (3.1 - 1.6)	1.6 (4.1 - 2.4)	0	2.1 (2.4 - 0.3)	0	3.6 (4.5 - 0.9)	1.5 (3.1 - 1.6)	7.3 (11.0 - 3.6)
		1.2 (2.9 - 1.8)	1.2 (2.9 - 1.7)	0	0	0	0	1.2 (2.9 - 1.8)	1.2 (2.9 - 1.7)
		14.4 (14.5 - 0.1)		3.5 (4.2 - 0.7)		-1.5 (0.4 - 1.9)		16.4 (19.1 - 2.7)	
East Indian (>0 northward)		5.6 (23.2 - 17.6)	5.4 (23.5 - 18.1)	4.4 (9.1 - 4.7)	4.1 (9.4 - 5.4)	-3.7 (8.6 - 12.4)	-2.7 (10.0 - 12.7)	6.3 (40.9 - 34.7)	6.7 (42.9 - 36.2)
		6.0 (23.8 - 17.8)	4.8 (22.8 - 18.0)	4.7 (9.9 - 5.2)	4.9 (8.5 - 3.6)	-3.7 (9.6 - 13.3)	-1.1 (7.0 - 8.1)	7.0 (43.3 - 36.3)	8.7 (38.3 - 29.7)
		5.4 (23.2 - 17.8)	4.9 (24.0 - 19.0)	4.9 (9.6 - 4.7)	4.6 (9.7 - 5.1)	-3.9 (9.1 - 13.1)	-3.3 (9.1 - 12.3)	6.4 (41.9 - 35.6)	6.3 (42.8 - 36.4)
		-7.2 (44.4 - 51.6)		-5.2 (8.3 - 13.5)		-1.6 (12.7 - 14.2)		-14.0 (65.4 - 79.3)	
Indo-Asian (>0 Tethys to Indo-Pac.)		-8.9 (15.1 - 23.9)	-9.8 (14.2 - 24.0)	1.2 (2.9 - 1.6)	1.7 (3.1 - 1.4)	-2.6 (2.9 - 5.5)	0 (6.3 - 6.3)	-10.2 (20.9 - 31.0)	-8.1 (23.6 - 31.7)
		-9.2 (14.9 - 24.1)	-9.5 (16.1 - 25.6)	0.6 (3.0 - 2.3)	3.4 (4.2 - 0.8)	-2.7 (4.1 - 6.8)	-0.7 (2.8 - 3.4)	-11.3 (22.0 - 33.2)	-6.8 (74.7 - 61.1)
		-8.8 (15.8 - 24.6)	-9.6 (13.9 - 23.5)	1.7 (3.2 - 1.6)	3.7 (4.2 - 0.6)	-2.8 (2.9 - 5.8)	-4.3 (2.4 - 6.7)	-9.9 (21.9 - 32.0)	-10.3 (20.5 - 30.8)
		6.4 (51.9 - 45.5)		0.7 (14.8 - 14.1)		-4.4 (13.2 - 17.6)		2.8 (79.9 - 77.2)	
Indonesian (>0 eastward)		11.4 (58.2 - 46.8)	11.1 (59.8 - 48.7)	4.7 (11.6 - 6.9)	4.9 (12.0 - 7.0)	-7.4 (8.1 - 15.5)	-3.7 (11.1 - 14.8)	8.8 (77.9 - 69.2)	12.3 (82.9 - 70.5)
		11.9 (61.6 - 49.7)	9.7 (54.8 - 45.1)	5.1 (12.3 - 7.2)	6.4 (12.7 - 6.3)	-7.4 (9.1 - 16.6)	-2.4 (7.2 - 9.7)	9.6 (83.0 - 73.5)	13.7 (74.7 - 61.1)
		10.7 (57.5 - 46.8)	10.4 (56.5 - 46.1)	5.4 (11.9 - 6.5)	6.6 (12.8 - 6.2)	-7.7 (8.3 - 16.0)	-8.7 (6.6 - 15.3)	8.3 (77.7 - 69.3)	8.4 (75.9 - 67.6)
		-22.9 (0.9 - 23.8)		-3.6 (0 - 3.7)		-1.7 (0 - 1.7)		-28.2 (0.9 - 29.2)	
Mediterranean (>0 eastward)		-6.6 (0.5 - 7.1)	-6.8 (0.4 - 7.2)	0.2 (0.4 - 0.2)	0.1 (0.3 - 0.2)	0.2 (0.2 - 0)	0.2 (0.2 - 0)	-6.3 (1.1 - 7.3)	-6.5 (0.9 - 7.4)
		-6.9 (0.5 - 7.3)	-6.5 (0.5 - 7.0)	0.2 (0.4 - 0.2)	0.2 (0.4 - 0.2)	0.2 (0.2 - 0)	0.1 (0.1 - 0)	-6.5 (1.1 - 7.5)	-6.2 (1.0 - 7.2)
		-6.9 (0.4 - 7.3)	-9.1 (1.9 - 11.0)	0.2 (0.4 - 0.2)	0.5 (3.4 - 2.9)	0.1 (0.1 - 0)	-4.7 (0.9 - 5.7)	-6.5 (0.9 - 7.5)	-13.3 (6.2 - 19.6)
		-1.4 (1.4 - 2.8)		1.7 (2.6 - 0.9)		-0.7 (0.1 - 0.8)		-0.4 (4.1 - 4.5)	
South African (>0 eastward)		3.0 (13.4 - 10.3)	1.8 (14.1 - 12.3)	2.6 (8.2 - 5.7)	1.9 (6.9 - 5.0)	-4.1 (3.2 - 7.3)	0.6 (3.9 - 3.3)	1.5 (24.8 - 23.3)	4.4 (24.9 - 20.6)
		3.1 (13.4 - 10.4)	2.3 (12.4 - 10.1)	2.7 (8.6 - 5.9)	3.9 (8.2 - 4.4)	-4.2 (3.4 - 7.6)	1.0 (3.9 - 2.9)	1.4 (25.4 - 23.9)	7.2 (24.5 - 17.4)
		2.7 (12.7 - 10.0)	3.3 (14.7 - 11.5)	3.7 (8.5 - 5.1)	4.0 (8.6 - 4.6)	-4.3 (3.1 - 7.5)	0.3 (3.5 - 3.2)	1.7 (24.3 - 22.6)	7.6 (26.8 - 19.3)
		1.8 (6.4 - 4.6)		-0.8 (1.1 - 1.9)		-0.1 (0.2 - 0.3)		0.9 (7.7 - 6.8)	
South Atlantic (>0 northward)		0 (15.2 - 15.2)	0.8 (15.3 - 14.5)	-2.5 (3.9 - 6.4)	-1.0 (3.6 - 4.6)	3.1 (4.1 - 1.0)	-2.1 (2.0 - 4.0)	0.6 (23.2 - 22.6)	-2.3 (20.9 - 23.1)
		0.2 (15.3 - 15.1)	0 (14.8 - 14.8)	-2.6 (4.0 - 6.7)	-1.5 (4.2 - 5.7)	3.3 (4.6 - 1.2)	2.3 (3.2 - 0.9)	0.8 (23.8 - 23.0)	0.8 (22.2 - 21.4)
		0.1 (15.2 - 15.0)	-0.6 (15.4 - 15.9)	-3.5 (3.6 - 7.1)	-3.2 (3.7 - 6.9)	3.5 (4.7 - 1.2)	-1.9 (1.7 - 3.6)	0.1 (23.5 - 23.3)	-5.7 (20.8 - 26.4)
		-24.7 (0.9 - 25.6)		-4.2 (0 - 4.3)		0		-28.9 (0.9 - 29.9)	
South China (>0 eastward)		0	0	0	0	0	0	0	0
		0	0	0	0	0	0	0	0
		0	0	0	0	0	0	0	0
		-20.7 (10.2 - 30.9)		-3.1 (3.5 - 6.7)		-0.4 (3.7 - 4.1)		-24.3 (17.4 - 41.7)	
Tethys (>0 Tethys to Indo-Pac.)		-6.3 (7.8 - 14.1)	-6.5 (7.5 - 14.0)	1.5 (2.9 - 1.4)	1.5 (2.7 - 1.3)	0 (1.2 - 1.2)	0 (1.3 - 1.3)	-4.8 (11.9 - 16.7)	-5.0 (11.5 - 16.6)
		-6.2 (9.0 - 15.1)	-6.9 (7.3 - 14.2)	1.1 (2.4 - 1.3)	2.2 (3.8 - 1.6)	0 (1.7 - 1.7)	0 (1.2 - 1.2)	-5.0 (13.1 - 18.1)	-4.7 (12.3 - 17.0)
		-6.3 (8.2 - 14.5)	-8.1 (4.4 - 12.5)	1.5 (3.0 - 1.4)	1.8 (2.8 - 1.0)	0 (1.2 - 1.2)	-5.4 (1.5 - 6.9)	-4.8 (12.4 - 17.1)	-11.7 (8.7 - 20.4)
West Indian (>0 northward)									
	Ceno.	-16.6 (0 - 16.6)		0		0		-16.6 (0 - 16.6)	
Maas. Western side		-6.8 (1.7 - 8.5)	-7.7 (1.7 - 9.4)	0.5 (0.8 - 0.3)	-0.7 (0.3 - 1.0)	-0.1 (0.1 - 0.2)	0 (0.1 - 0.1)	-6.4 (2.6 - 9.0)	-8.4 (2.1 - 10.5)
		-7.3 (1.7 - 8.9)	-7.1 (1.7 - 8.8)	0.3 (0.7 - 0.4)	0.7 (1.0 - 0.3)	-0.1 (0.1 - 0.2)	0.1 (0.1 - 0)	-7.1 (2.5 - 9.5)	-6.4 (2.8 - 9.1)
		-7.0 (1.8 - 8.7)	-6.1 (1.8 - 7.9)	1.0 (1.3 - 0.3)	1.1 (1.2 - 0.1)	-0.1 (0.1 - 0.1)	0.1 (0.1 - 0)	-6.1 (3.2 - 9.2)	-5.0 (3.1 - 8.0)
Maas. Eastern side		3.5 (5.1 - 1.6)	3.9 (5.4 - 1.5)	-0.6 (0.6 - 1.2)	0.8 (1.6 - 0.8)	-1.2 (0.3 - 1.5)	1.3 (1.9 - 0.6)	1.6 (6.0 - 4.3)	6.0 (8.9 - 2.9)
		3.7 (5.3 - 1.5)	3.7 (5.3 - 1.5)	-0.7 (0.5 - 1.3)	1.0 (1.4 - 0.4)	-1.5 (0.3 - 1.7)	0.1 (0.4 - 0.3)	1.6 (6.1 - 4.5)	4.9 (7.1 - 2.2)
		3.5 (5.0 - 1.5)	3.9 (5.4 - 1.6)	-0.6 (0.6 - 1.2)	0.8 (1.7 - 0.9)	-1.5 (0.2 - 1.7)	1.7 (2.4 - 0.7)	1.4 (5.8 - 4.4)	6.3 (9.5 - 3.2)

Simulation: Cenomanian Maastrichtian Deep Caribbean Seaway
Maastrichtian 2x CO₂ Deep Drake Passage
Deep Labrador Seaway Deep Neotethys Seaway

Table S1. Water transport across major oceanic sections (shown on Figs. 5 and 6) for each simulation. For each section is shown the direction of the positive transport across the gateway. There is

bidirectional flow, i.e. positive and negative water fluxes, across most sections. The sum of positive and negative fluxes across a section gives the net water transport across the section. The net water transport is shown for three depth ranges (upper, intermediate and deep ocean) and for the total vertical extension of the section. The summed positive and negative fluxes for the depth intervals considered are also shown in parentheses. The sign of the net water transport therefore gives the direction of the larger water flux across a section. Positive and negative fluxes are represented on Figs. 5 and 6 for the intermediate and deep ocean respectively.

24
25
26
27
28
29
30
31
32
33
34

	Cenomanian				Maastrichtian			
<u>Total runoff supply (mSv)</u> <u>Total basin area (10⁶ km²)</u>	Pacific	Atlantic	Indo-Neo- tethys	Indo-Atlantic- Neotethys	Pacific	Atlantic	Indo-Neo- tethys	Indo-Atlantic- Neotethys
Global	<u>833</u> 221.84	<u>654</u> 46.46	<u>945</u> 100.57	<u>1599</u> 147.03	<u>792</u> 212.27	<u>864</u> 58.97	<u>931</u> 94.96	<u>1796</u> 153.93
Southern Hemisphere high-latitudes	<u>130</u> 19.95	<u>54</u> 5.59	<u>195</u> 8.03	<u>248</u> 13.63	<u>129</u> 17.61	<u>55</u> 9.27	<u>211</u> 11.11	<u>266</u> 20.38
Northern Hemisphere high-latitudes	<u>130</u> 15.49	<u>175</u> 6.79	<u>72</u> 1.37	<u>248</u> 8.15	<u>169</u> 15.04	<u>160</u> 3.53	<u>47</u> 1.75	<u>207</u> 5.28
Mid- and low- latitudes	<u>573</u> 186.4	<u>425</u> 34.08	<u>678</u> 91.17	<u>1103</u> 125.25	<u>494</u> 179.62	<u>649</u> 46.18	<u>674</u> 82.1	<u>1323</u> 128.28

Table S2. Total runoff freshwater supply (mSv) for the Cenomanian and Maastrichtian simulations. The Pacific, Atlantic and Indo-Neotethyan basins are defined as shown on Fig. S3. Southern and northern high-latitudes are defined as latitudes < 50°S and > 50°N respectively.

35

Site	Location	Paleolatitude	Paleolongitude	Paleodepth (m)	Average ϵ_{Nd}	References
765	Argo Abyssal Plain	40°S	105°E	5000	-7.9	MT12, GL92
763	Central Exmouth Plateau	44°S	100°E	500	-9.8	LH12, MT12, V13, GL92
766	Gascoyne Abyssal Plain	45°S	95°E	3000	-6.8	R10, MT12, GL92
258	Naturaliste Plateau	57°S	85°E	2500 – 3000	-8.0	M16
1135	Southern Kerguelen Plateau	55°S	72°E	1300 – 2000	-7.9	LH12
1138	Kerguelen Plateau	52°S	70°E	500 – 1500	-5.6	MT12
551	Goban Spur	40°N	2°W	1500	-7.1	M12, M85
530	SE Angola Basin	30°S	4°W	> 2000	-7.5	R10
530	SE Angola Basin	31°S	5°W	3000	-7.7	MT13
361	Cape Basin	45°S	5°W	4000	-6.1	MT13
367	Cape Verde	17°N	18°W	> 2000	-9.0	M12
700	East Georgia Basin	52°S	18°W	1500 – 2000	-7.7	M16
1276	Newfoundland Margin	35°N	22°W	> 2000	-6.8	RV12
511	Falkland Plateau	54°S	25°W	> 1000	-5.2	R10
511	Falkland Basin	52°S	26°W	1800	-5.1	MT13
1261	Demerara Rise	6°N	29°W	1000 – 1500	-13.0	M12
1260	Demerara Rise	8°N	31°W	1000 – 1500	-13.5	ML08, ML11, M12, JB10
1258	Demerara Rise	9°N	32°W	1000 – 1500	-13.5	ML08, ML11, M12, JB10
386	Bermuda Rise	27°N	35°W	> 2000	-6.8	M12, RV12
1050	Blake Nose	26°N	42°W	1000 – 2000	-5.2	M12
1208	Shatsky Rise	15°N	154°W	1500 – 2000	-3.4	MT12

Table S3. Cenomanian ϵ_{Nd} compilation based on Moiroud et al. (2016). The ϵ_{Nd} values are averaged between 100 Ma and 90 Ma (see main text). GL92: Gradstein and Ludden (1992), JB10: Jiménez Berrocoso et al. (2010), LH12: Le Houedec et al. (2012), M12: Martin et al. (2012), M16: Moiroud et al. (2016), M85: Masson et al. (1985), ML08: MacLeod et al. (2008), ML11: MacLeod et al. (2011), MT12: Murphy and Thomas (2012), MT13: Murphy and Thomas (2013), R10: Robinson et al. (2010), RV12: Robinson and Vance (2012), V13: Voigt et al. (2013).

Site	Location	Paleolatitude	Paleolongitude	Paleodepth (m)	Average ϵ_{Nd}	References
765	Argo Abyssal Plain	40°S	105°E	5000	-10.2	MT12, GL92
762	Central Exmouth Plateau	44°S	100°E	750	-11.0	LH12, V13, GL92
766	Gascoyne Abyssal Plain	46°S	98°E	3000	-9.4	R10, MT12, GL92
1135	Southern Kerguelen Plateau	58°S	72°E	1300 – 2000	-9.6	LH12
1138	Kerguelen Plateau	55°S	70°E	500 – 1500	-8.5	MT12
758	Ninetyeast Ridge	47°S	50°E	1500 – 2000	-10.3	LH12
530	SE Angola Basin	30°S	1°W	> 2000	-10.0	R10
551	Goban Spur	37°N	5°W	2100	-9.9	M12, M85
690	Maud Rise	65°S	6°W	1800	-9.8	V13
525	Walvis Ridge	36°S	8°W	1000 – 1500	-3.5	V13
367	Cape Verde	15°N	20°W	> 2000	-13.4	M12
700	East Georgia Basin	52°S	20°W	1500 – 2000	-8.2	M16
1276	Newfoundland Margin	35°N	22°W	> 2000	-6.6	RV12
357	Rio Grande Rise	34°S	25°W	1500	-9.7	MT13
511	Falkland Plateau	54°S	29°W	> 1000	-8.7	R10
1261	Demerara Rise	3°N	29°W	1000 – 1500	-15.9	ML11, M12
1260	Demerara Rise	5°N	31°W	1000 – 1500	-15.2	ML08, ML11, M12
1258	Demerara Rise	6°N	32°W	1000 – 1500	-14.8	ML08, ML11, M12
386	Bermuda Rise	26°N	40°W	> 2000	-9.5	M12, RV12
1050	Blake Nose	30°N	54°W	1000 – 2000	-8.5	M12
152	Nicaraguan Rise	15°N	70°W	1500 – 2000	-5.7	M16
323	Bellingshausen Plateau	67°S	100°W	2000	-3.8	T14
596	South Pacific	45°S	120°W	5000	-5.6	T14
1186	Ontong-Java Plateau	15°S	132°W	2800	-5.1	H20
465	Southern Hess Rise	8°N	138°W	900	-3.8	H12
464	Northern Hess Rise	12°N	140°W	4000	-5.1	H12
883	Detroit Seamount	34°N	140°W	2000	2.4	H12, DT04
886	Chinook Trough	30°N	140°W	> 4400	-4.2	ML08
463	Mid-Pacific Mountains	5°S	145°W	1500 – 2000	-5.0	H20

1208	Shatsky Rise	15°N	154°W	3300	-4.0	H12
1209	Shatsky Rise	12°N	158°W	2000 – 3000	-4.3	T04, F05
1210	Shatsky Rise	10°N	160°W	2000 – 3000	-4.3	F05
1211	Shatsky Rise	8°N	162°W	2900	-4.2	T04

Table S4. Maastrichtian ϵ_{Nd} compilation based on Moiroud et al. (2016). The ϵ_{Nd} values are averaged between 75 Ma and 65 Ma (see main text). DT04: Doubrovine and Tarduno (2004), F05: Frank et al. (2005), GL92: Gradstein and Ludden (1992), H12: Hague et al. (2012), H20: Haynes et al. (2020), LH12: Le Houedec et al. (2012), M12: Martin et al. (2012), M16: Moiroud et al. (2016), M85: Masson et al. (1985), ML08: MacLeod et al. (2008), ML11: MacLeod et al. (2011), MT12: Murphy and Thomas (2012), MT13: Murphy and Thomas (2013), R10: Robinson et al. (2010), RV12: Robinson and Vance (2012), T04: Thomas (2004), T14: Thomas et al. (2014), V13: Voigt et al. (2013).

37

38

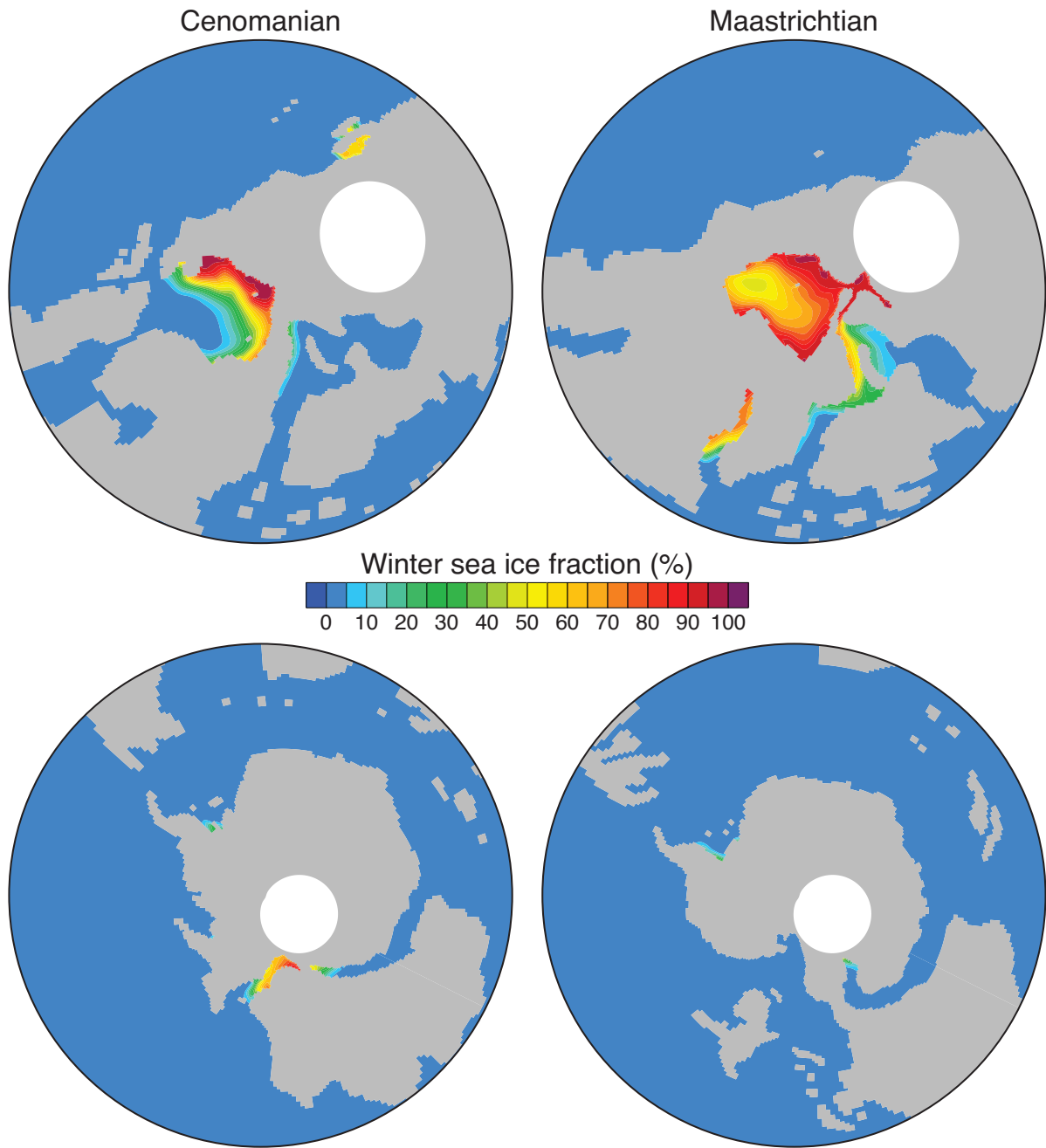


Figure S1. Mean winter sea ice fraction in the Cenomanian and Maastrichtian simulations.

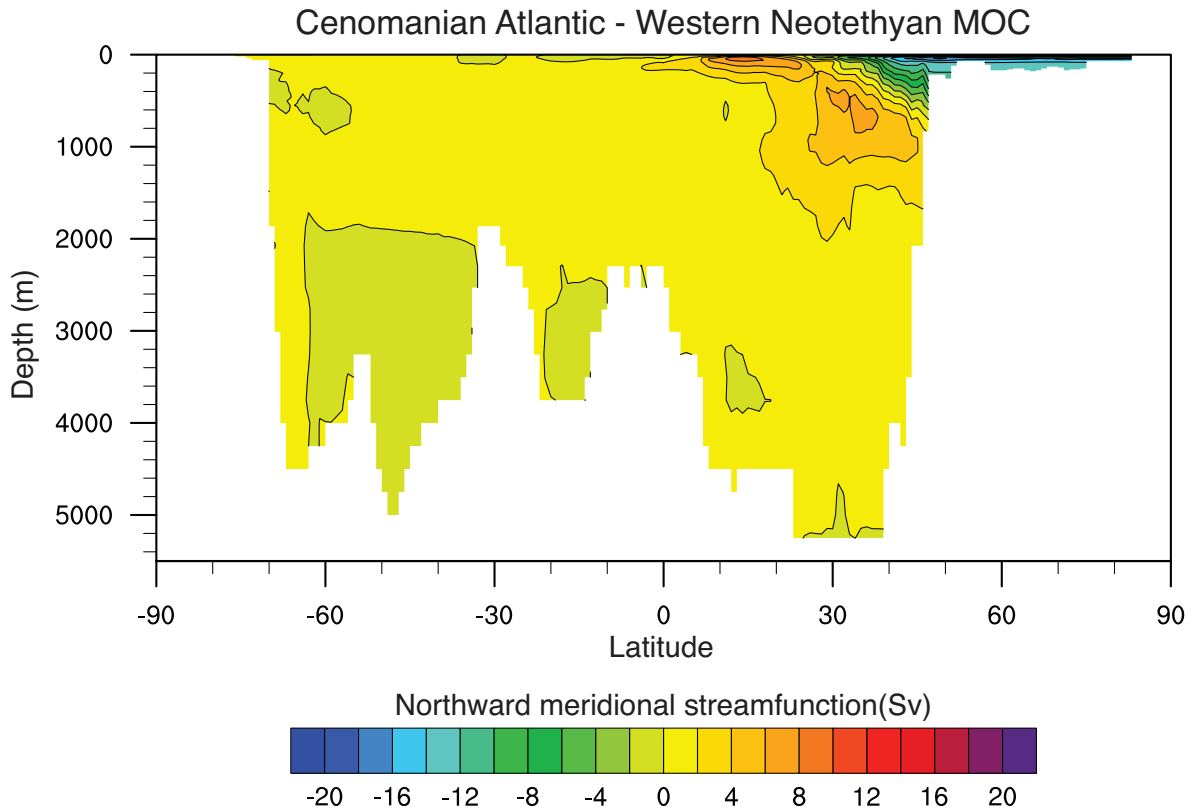


Figure S2. Meridional Overturning Circulation (Sv) in the Atlantic-Western Neotethyan basin of the Cenomanian simulation (Fig. S3).

40

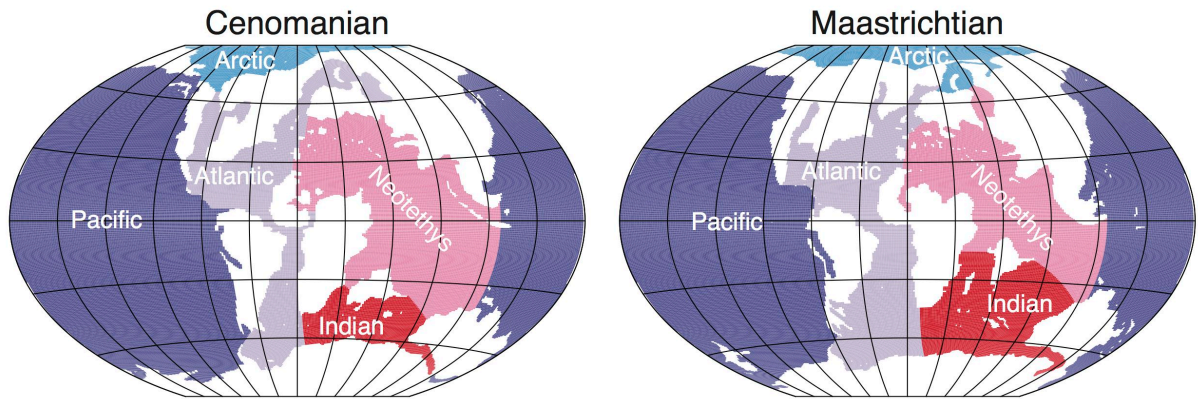


Figure S3. Configuration of the basin mask used in each simulation. In the text, the Neotethyan Ocean is sometimes split in a western Neotethyan Ocean (between Africa and Europe) and an eastern Neotethyan Ocean (between India and Asia).

41

Cenomanian intermediate circulation in the eastern Neotethyan and Indian Oceans

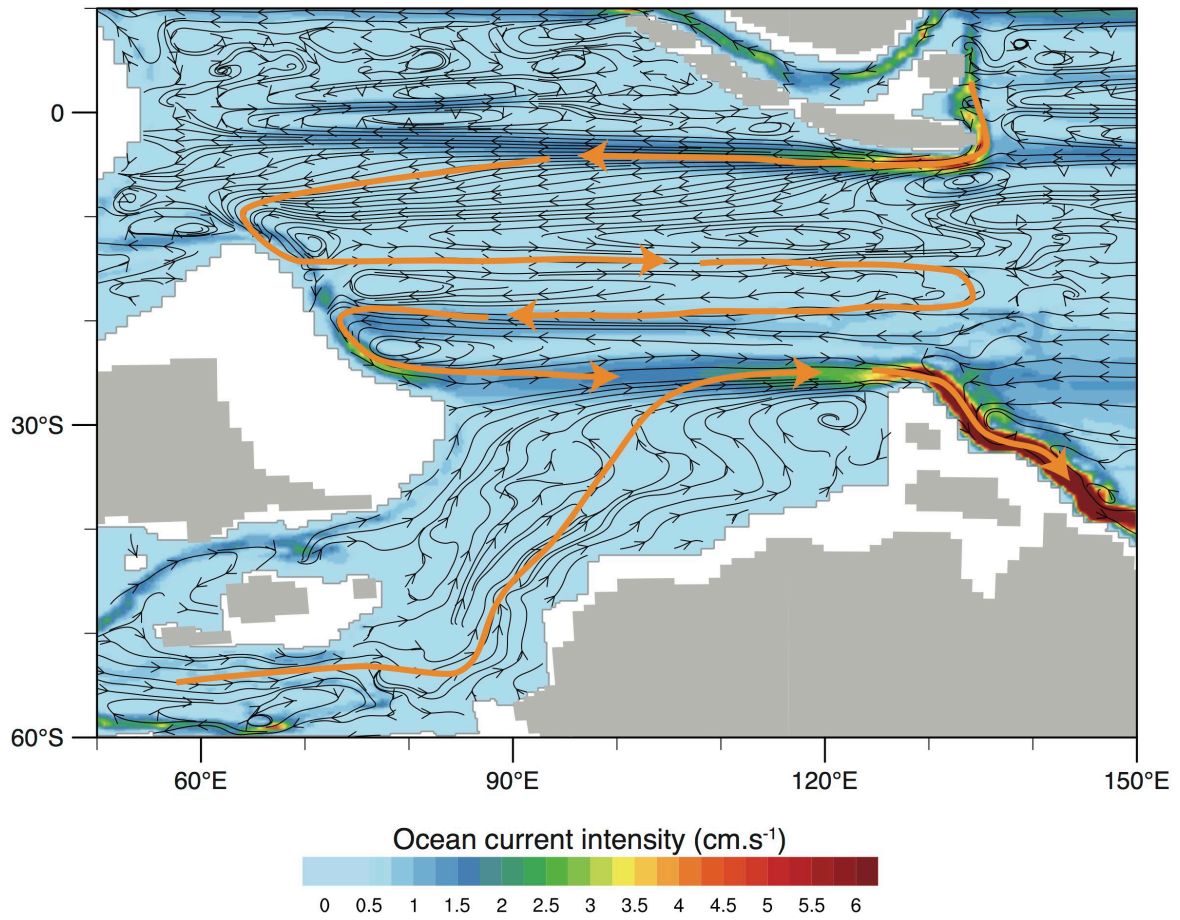


Figure S4. Cenomanian intermediate circulation (1000 m) in the eastern Neotethyan and Indian Oceans. Orange arrows represent major intermediate current systems in the eastern Neotethyan and Indian Oceans.

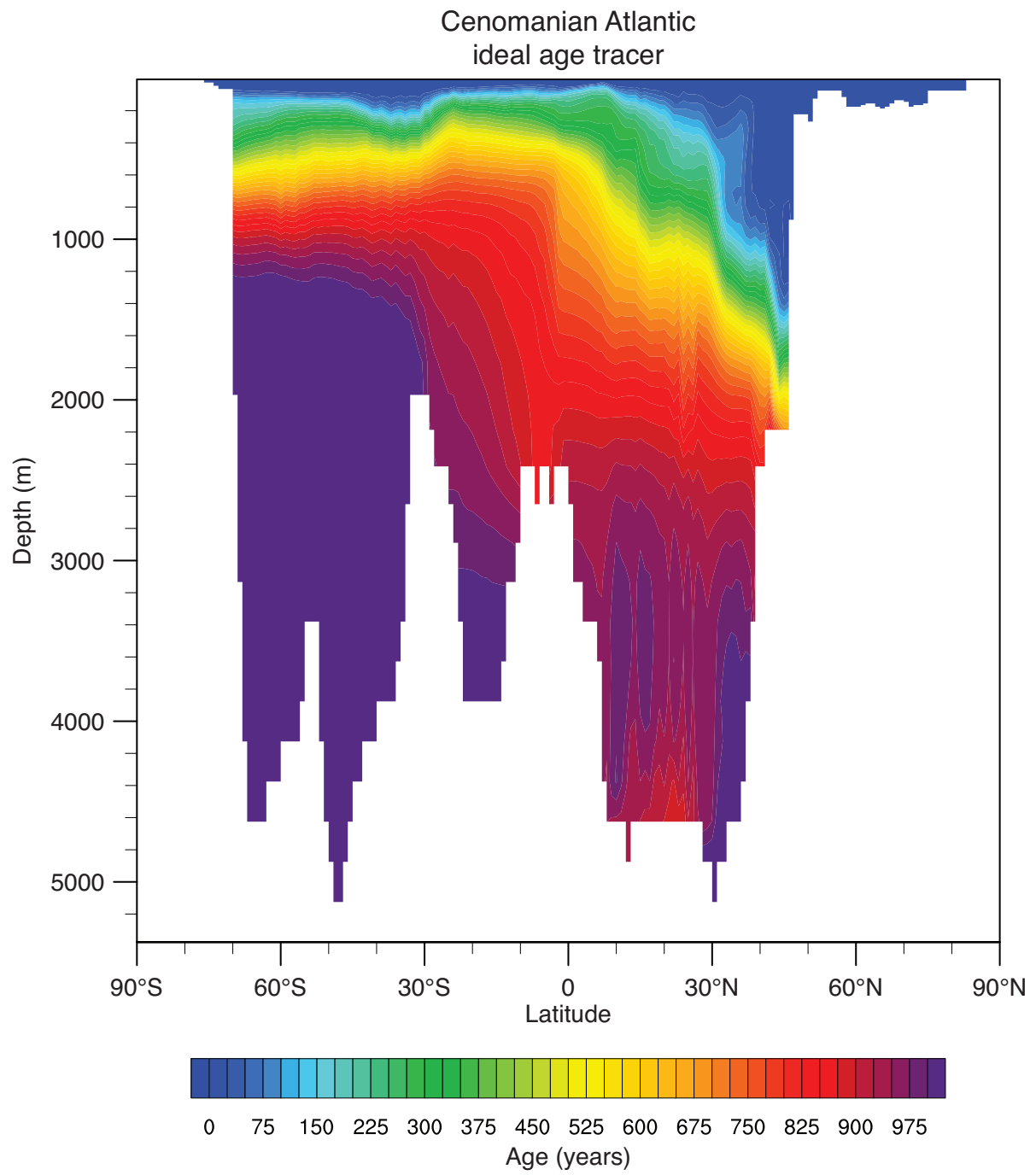


Figure S5. Cenomanian annual mean ideal age tracer in the Atlantic basin.

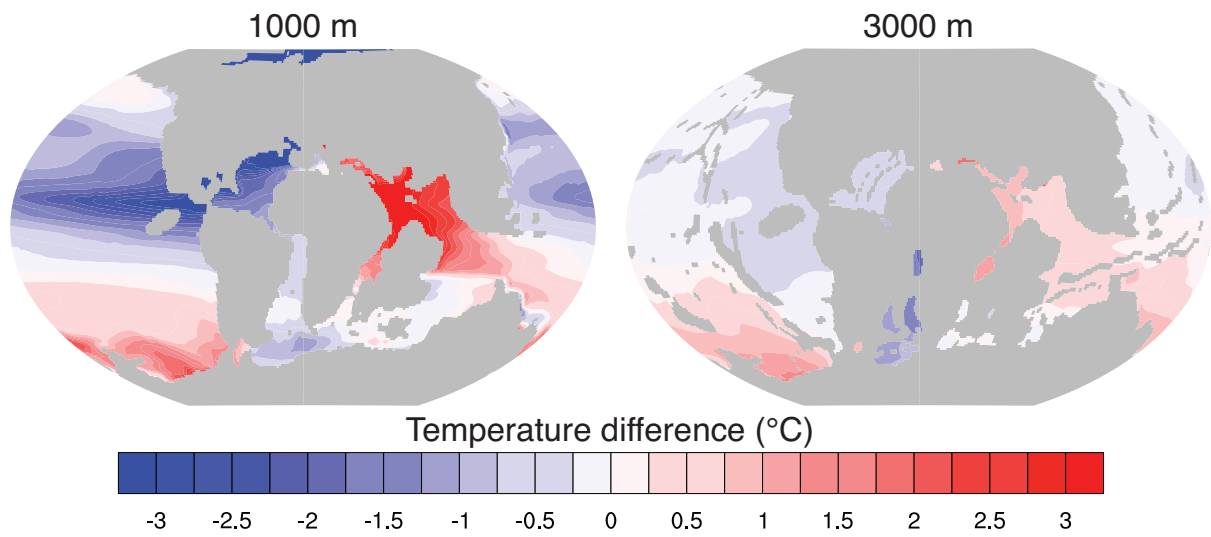


Figure S6. Intermediate (~1000 m) and deep (~3000 m) ocean temperature difference (°C) between the Maastrichtian and the Cenomanian simulations.

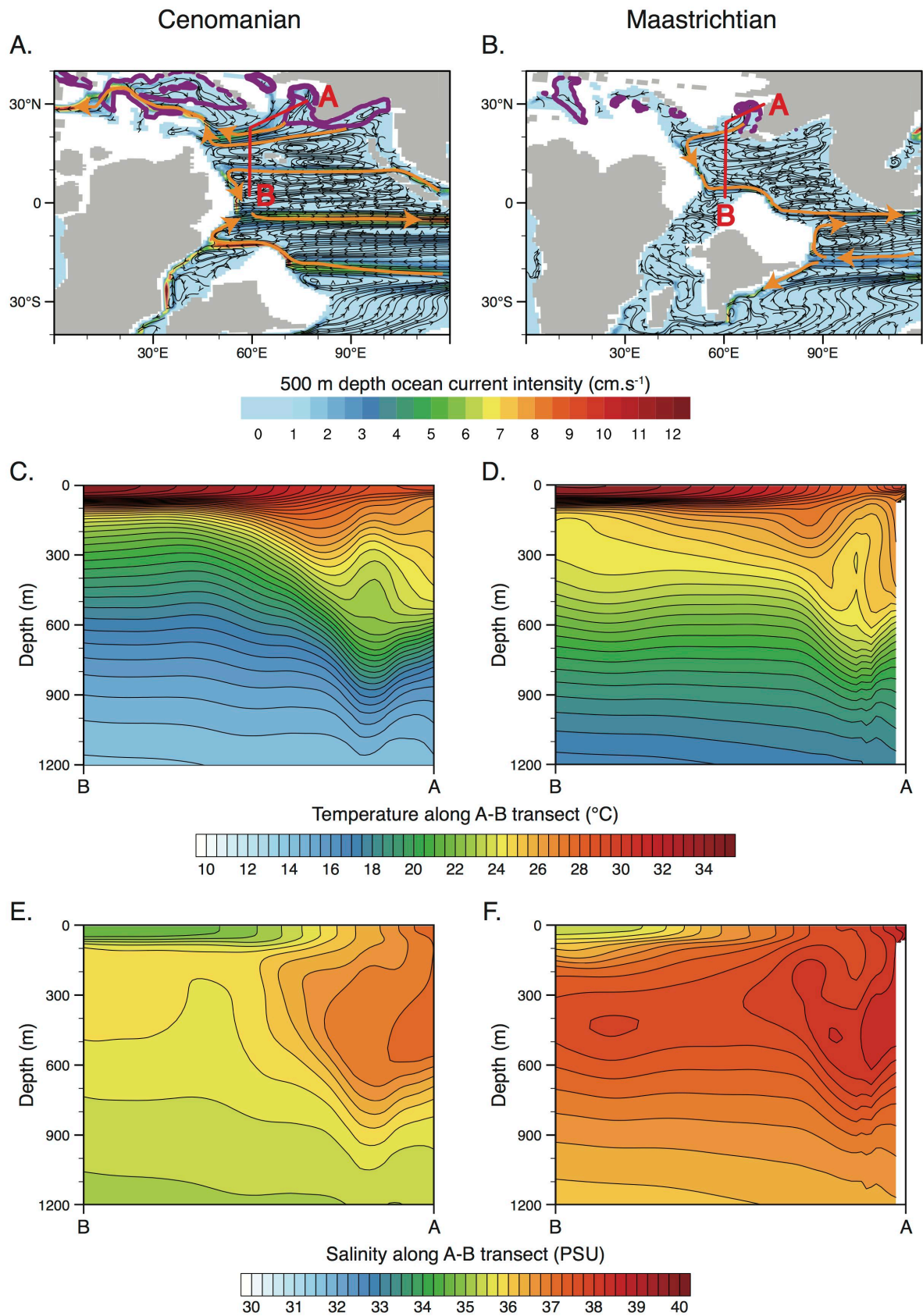


Figure S7. Upper intermediate (~ 500 m) ocean circulation for the Cenomanian (A) and Maastrichtian (B) simulations. Orange arrows represent major current systems in the

Neotethyan Ocean. Purple contours represent regions of late winter deepening of the mixed layer (200 m contours). Section A-B defines an ocean transect between regions of deeper winter MLD and the equatorial Neotethyan Ocean. (C and D) Ocean temperatures along the A-B transect for the Cenomanian and Maastrichtian respectively. (E and F) Same as C and D for the ocean salinity.

45

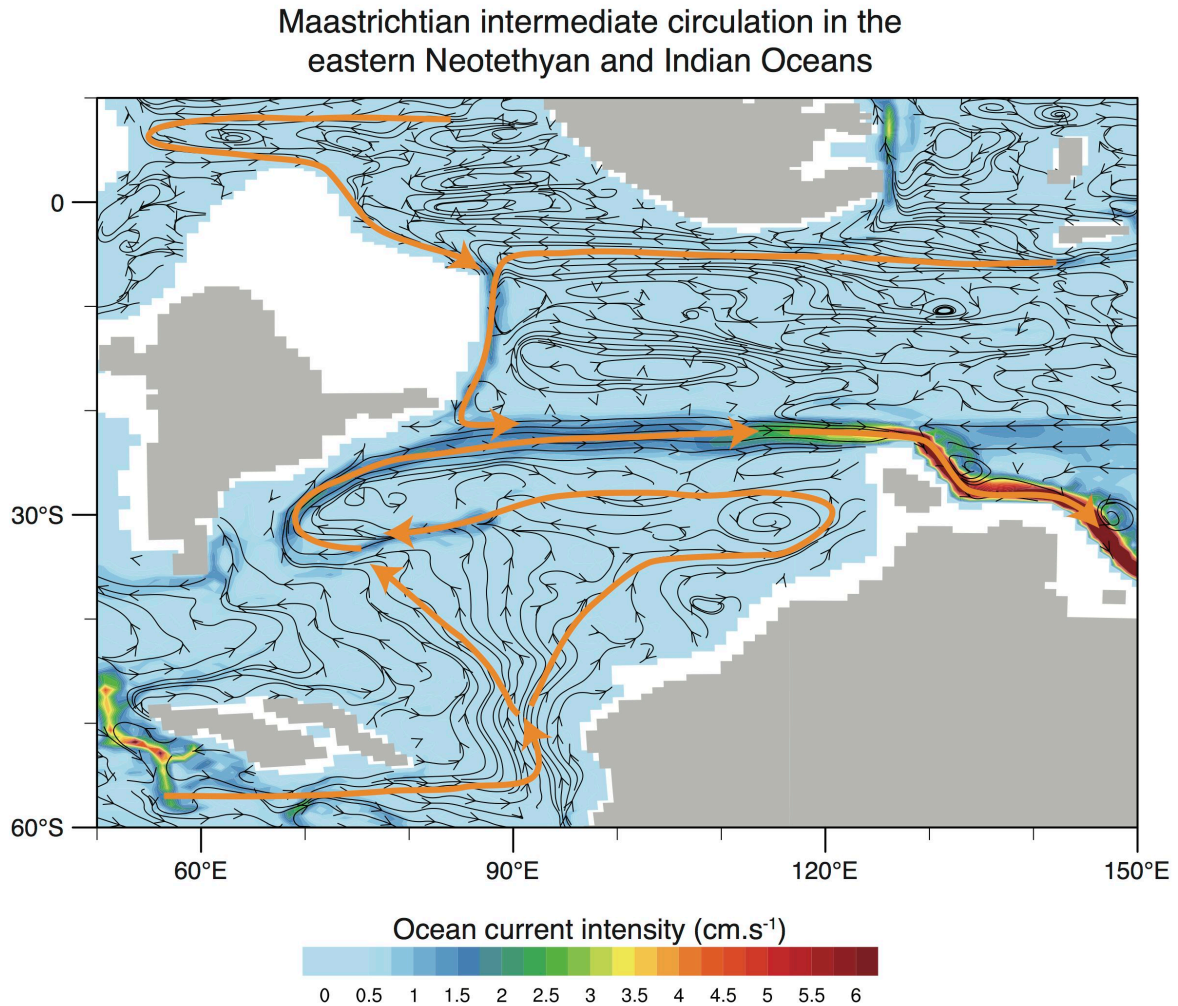


Figure S8. Maastrichtian intermediate circulation (1000 m) in the eastern Neotethyan and Indian Oceans. Orange arrows represent major intermediate current systems in the eastern Neotethyan and Indian Oceans.

46

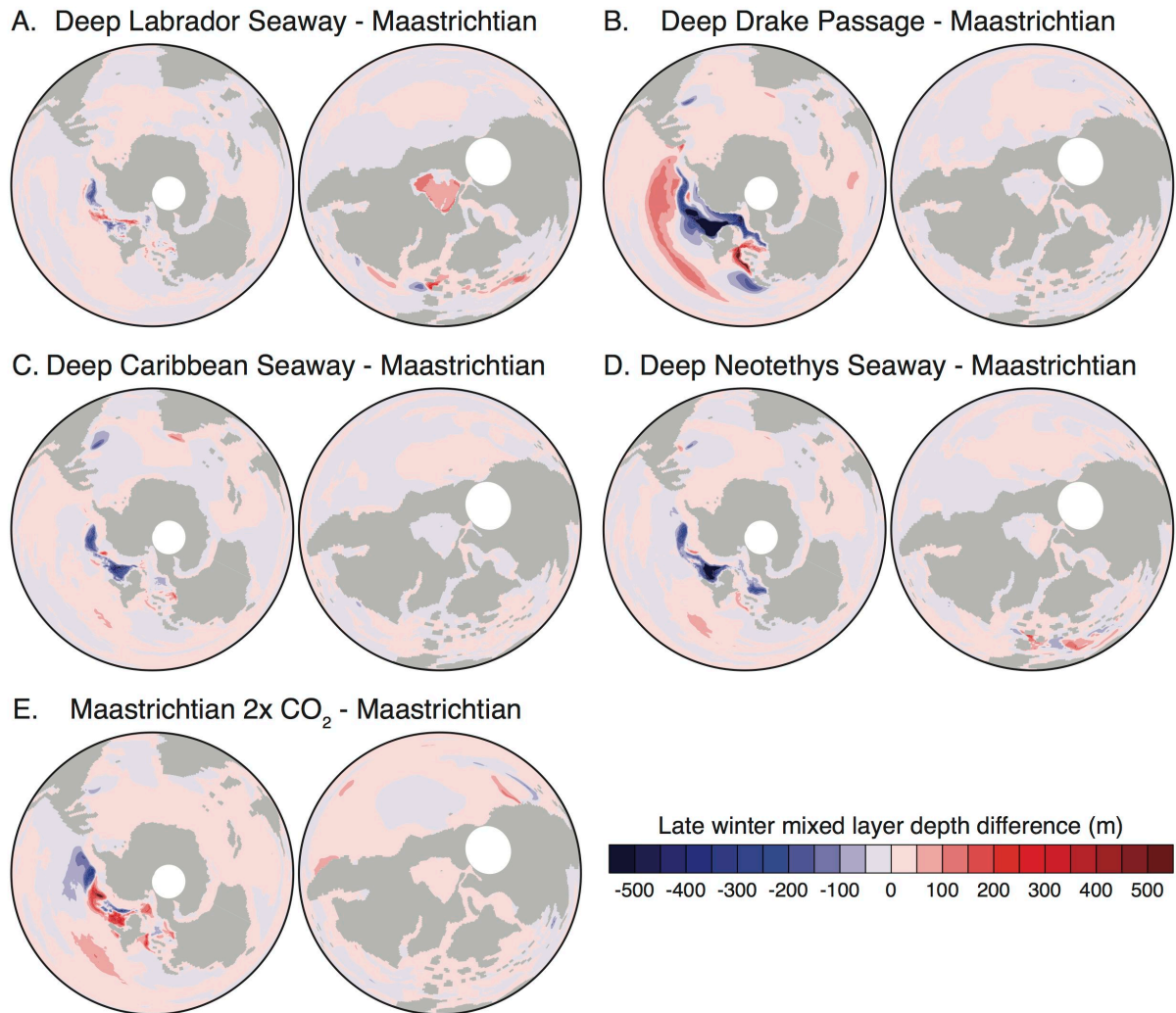


Figure S9. Southern and Northern hemispheres late winter maximal mixed layer depth difference (m) between the sensitivity experiments and the Maastrichtian simulation.

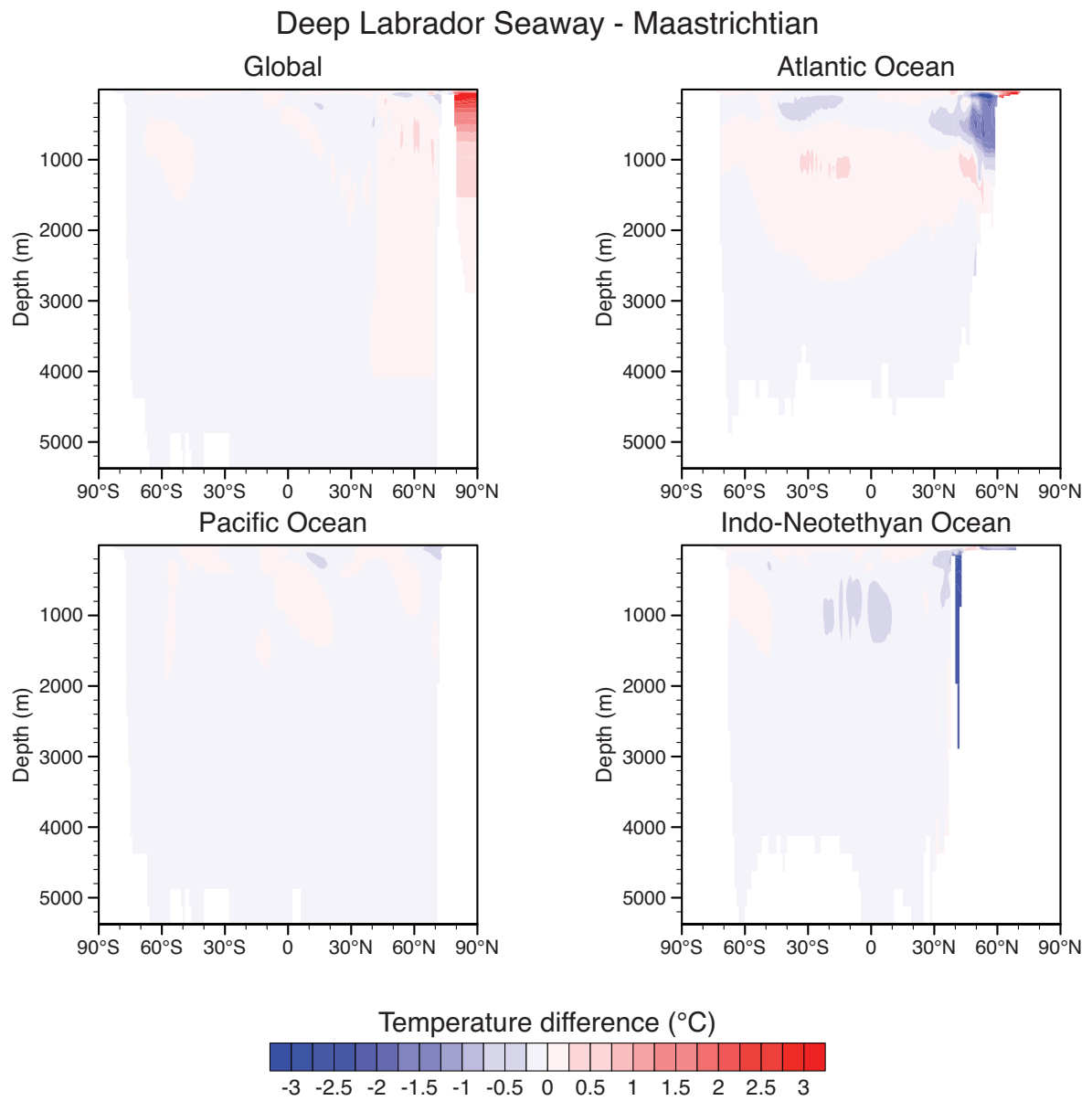


Figure S10. Zonally averaged ocean temperature changes (°C) in the different basins between the Deep Labrador Seaway and the Maastrichtian simulations.

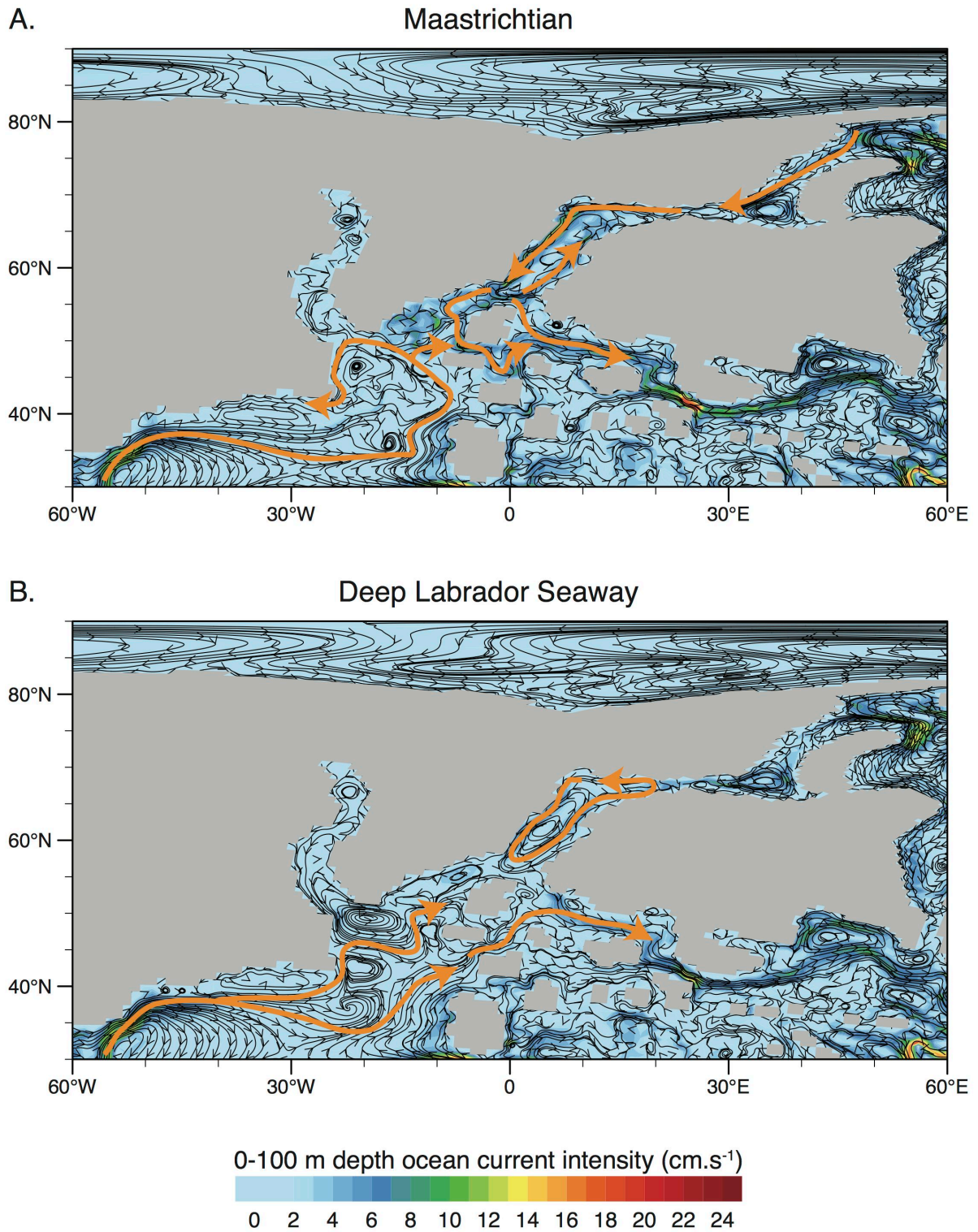


Figure S11. North Atlantic and northern Neotethys upper ocean circulation in (A) the Maastrichtian and (B) the Deep Labrador Seaway experiments. Orange arrows represent major current systems.

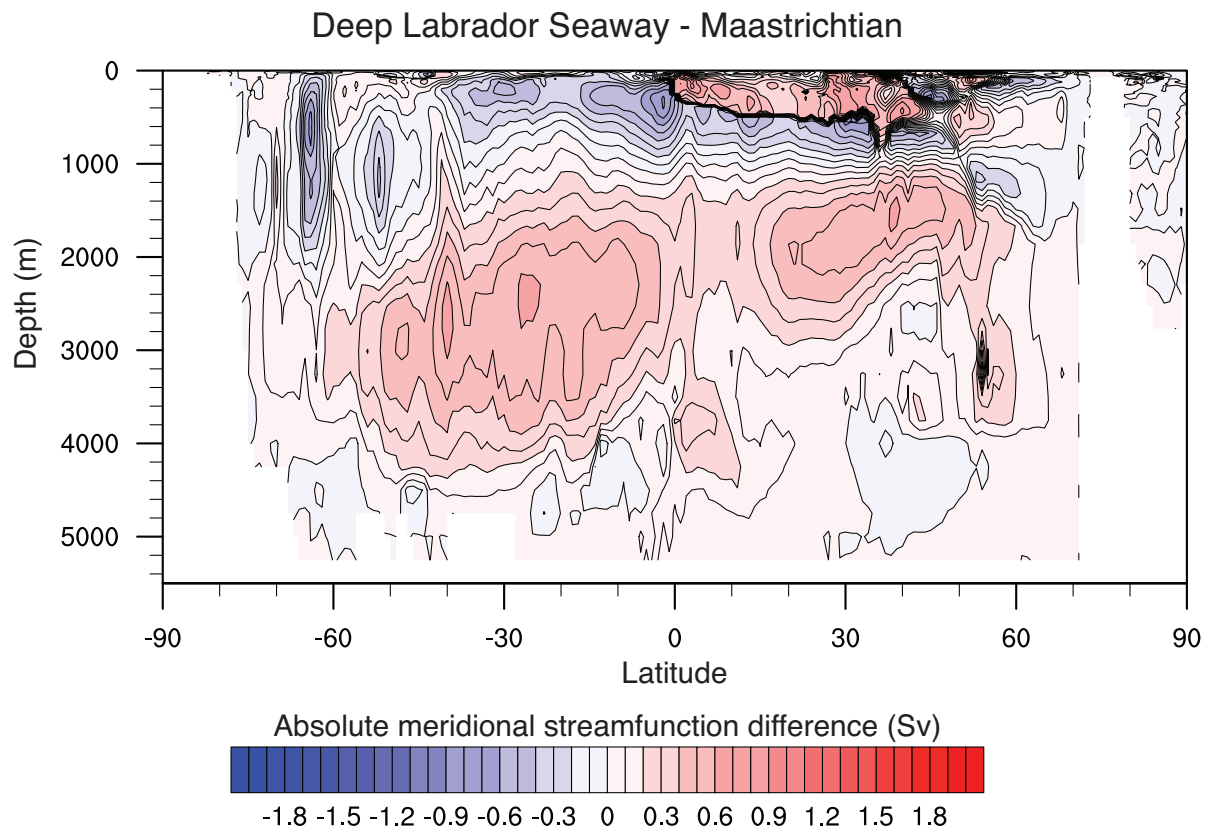


Figure S12. Difference of the absolute values of the global northward meridional streamfunction between the Deep Labrador Seaway and the Maastrichtian experiments. Positive values indicate a more vigorous circulation regardless of the sign of the global streamfunction in each simulation because the two global streamfunctions are very similar (Fig. 4B and 4C).

Deep Drake Passage - Maastrichtian

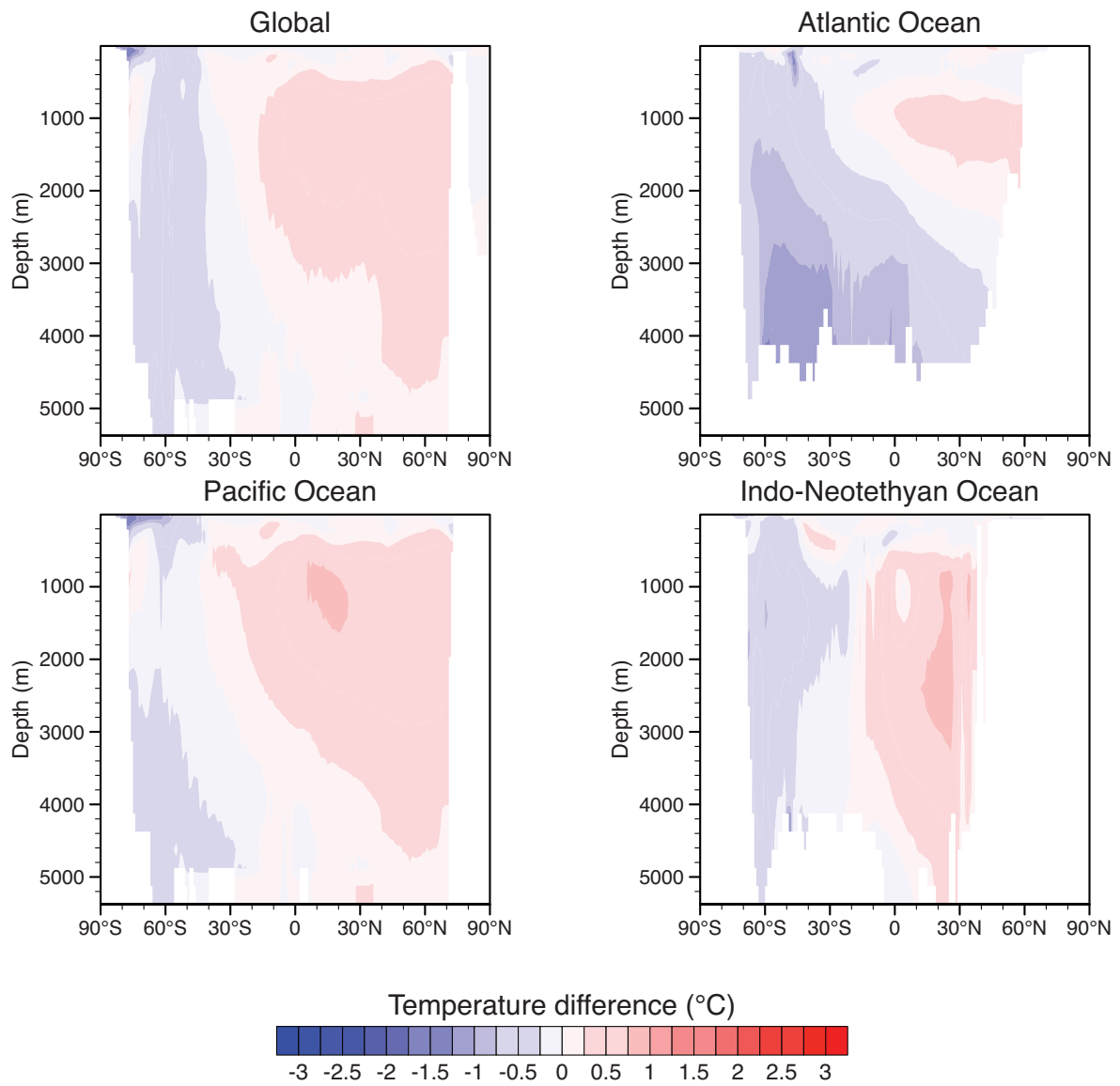


Figure S13. Zonally averaged ocean temperature changes ($^{\circ}\text{C}$) in the different basins between the Deep Drake Passage and the Maastrichtian simulations.

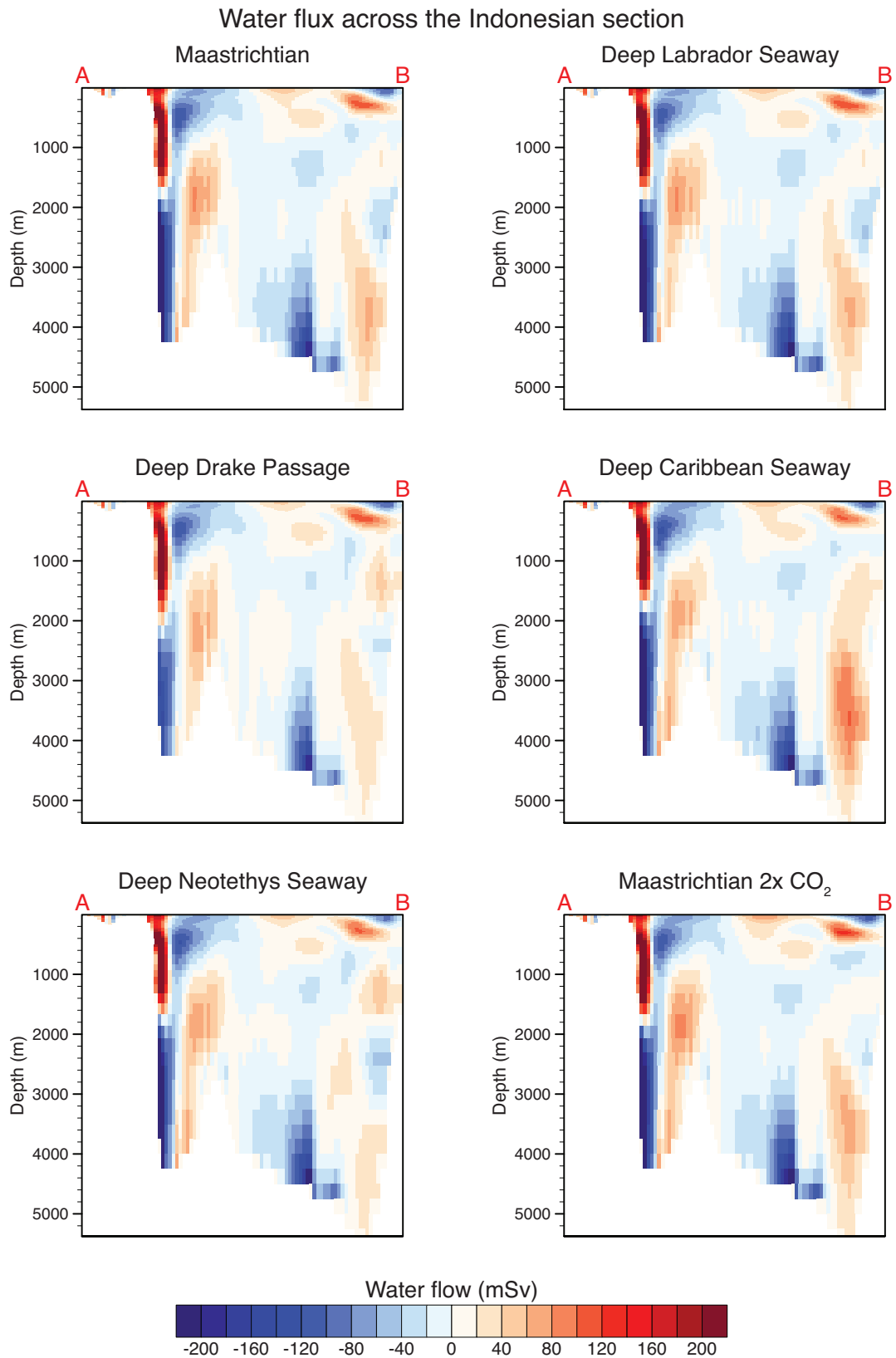


Figure S14. Water flux across the Indonesian section (mSv) for the Maastrichtian and Maastrichtian sensitivity experiments.

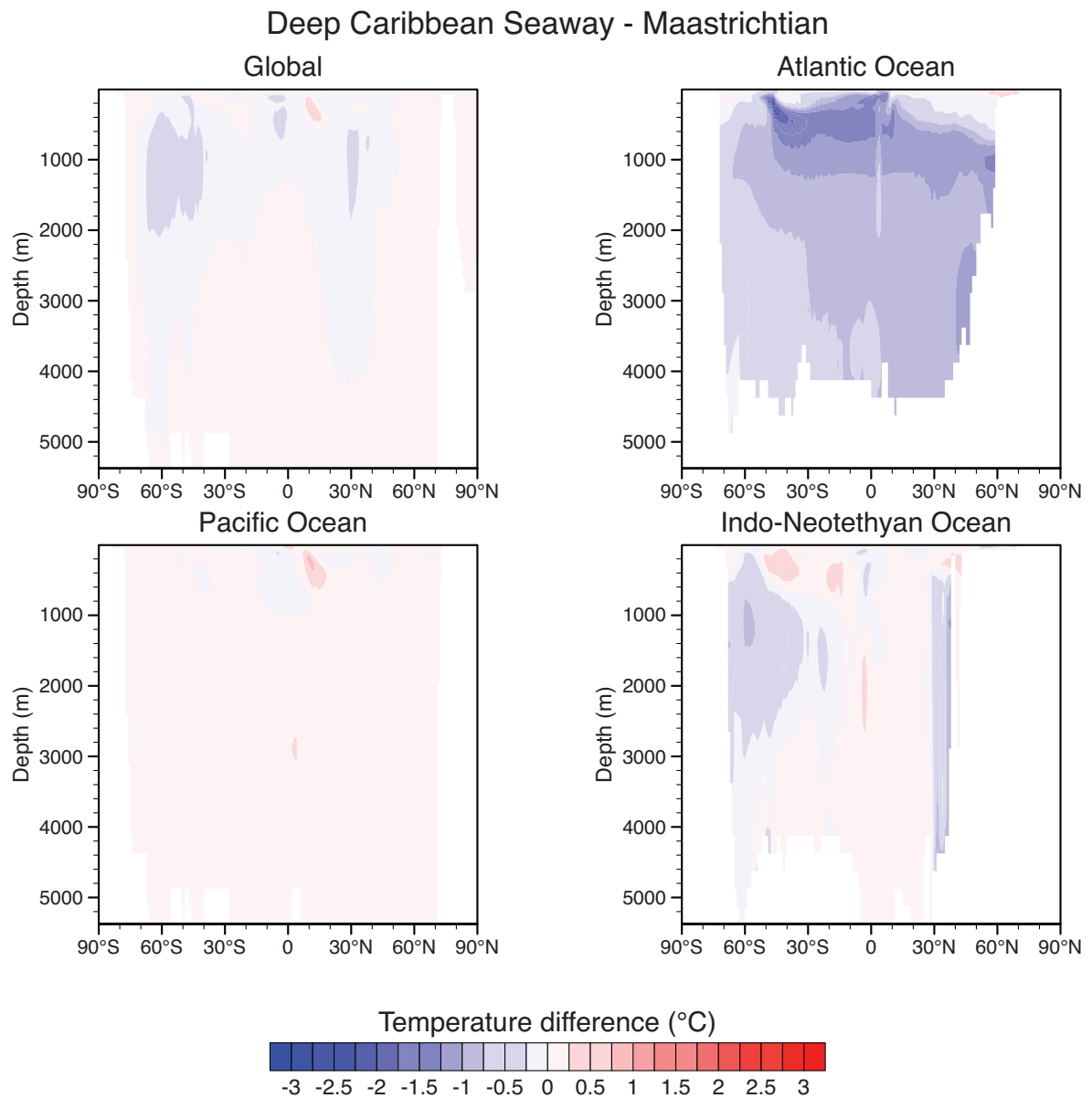


Figure S15. Zonally averaged ocean temperature changes (°C) in the different basins between the Deep Caribbean Seaway and the Maastrichtian simulations.

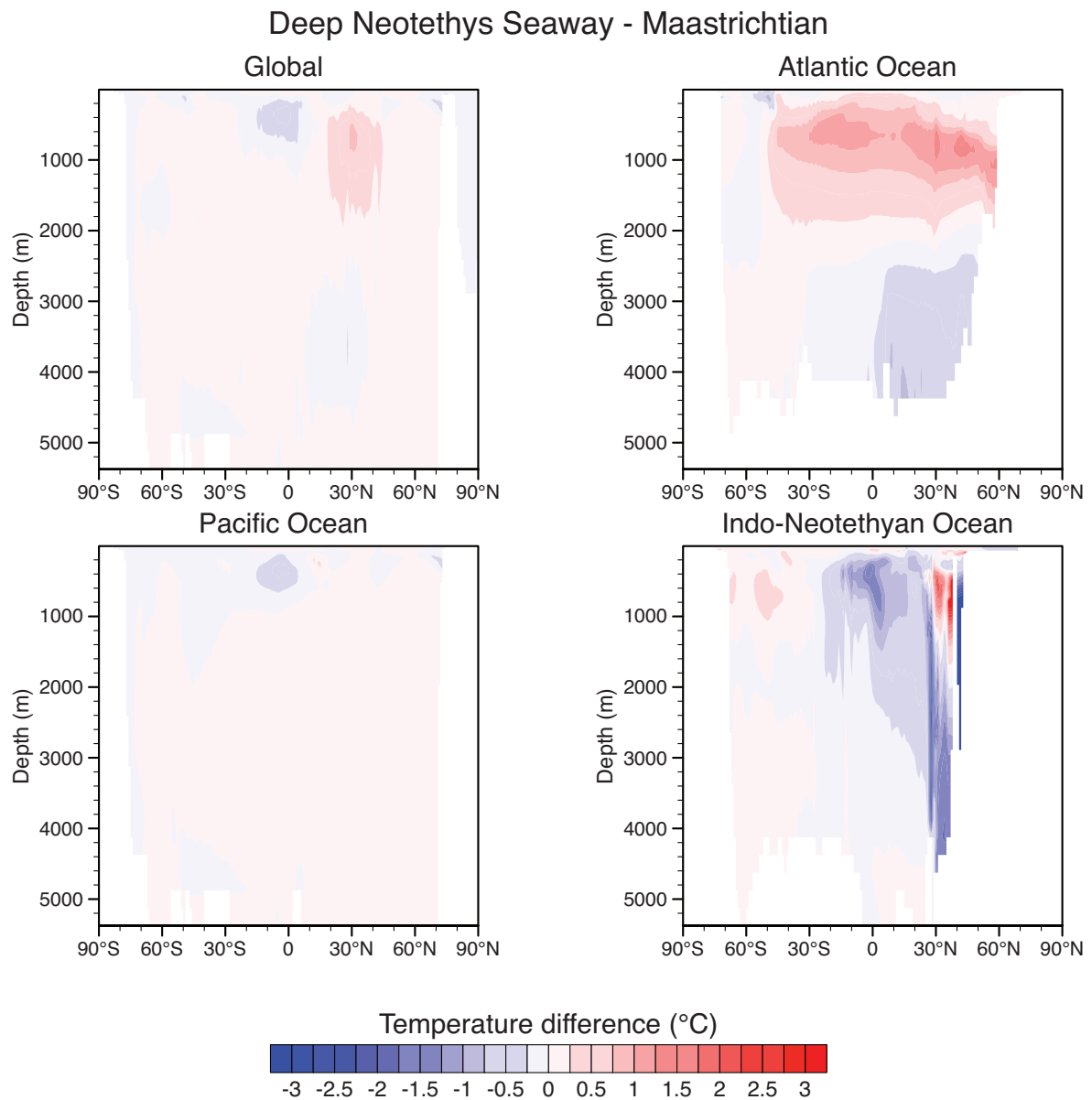


Figure S16. Zonally averaged ocean temperature changes (°C) in the different basins between the Deep Neotethys Seaway and the Maastrichtian simulations.

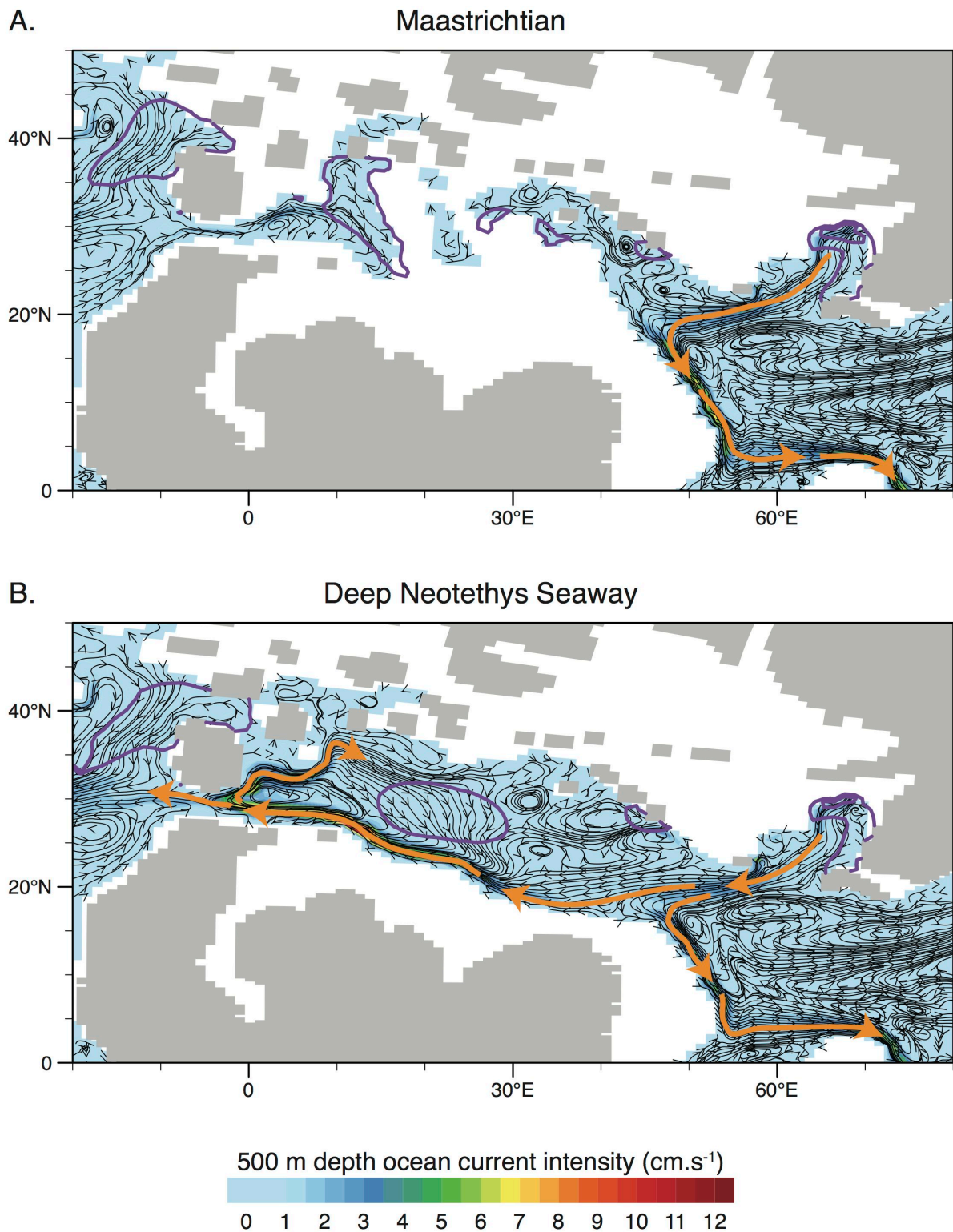


Figure S17. Neotethys upper intermediate (~ 500 m) ocean circulation in (A) the Maastrichtian and (B) the Deep Neotethys Seaway experiments. Orange arrows represent major current systems. Purple contours represent regions of late winter deepening of the mixed layer (200 m contours).

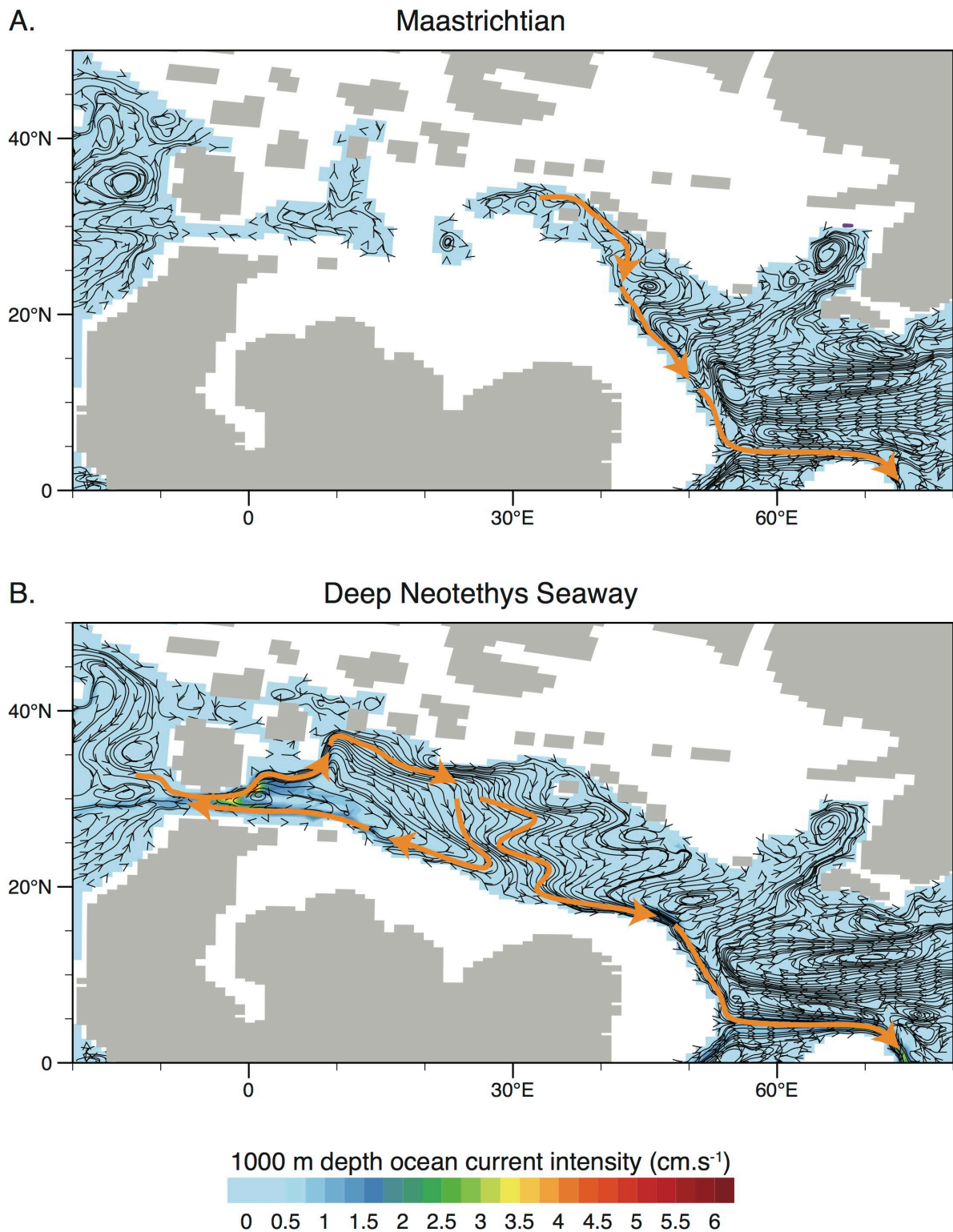


Figure S18. Neotethys deep intermediate (~ 1000 m) ocean circulation in (A) the Maastrichtian and (B) the Deep Neotethys Seaway experiments. Orange arrows represent major current systems.

Maastrichtian 2x CO₂ - Maastrichtian

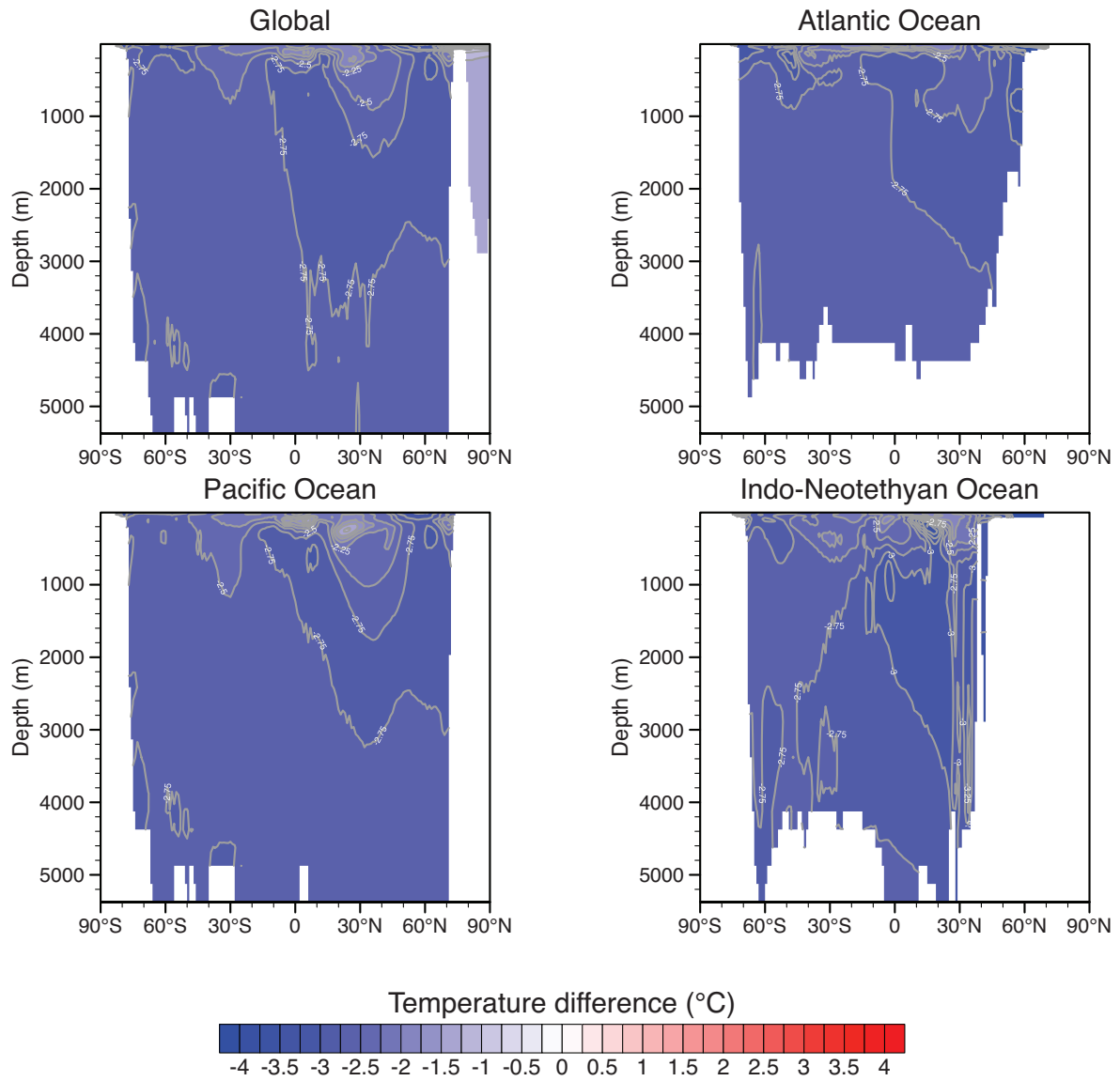


Figure S19. Zonally averaged ocean temperature changes (°C, 0.25 °C grey contours) in the different basins between the 2x CO₂ and the Maastrichtian simulations.

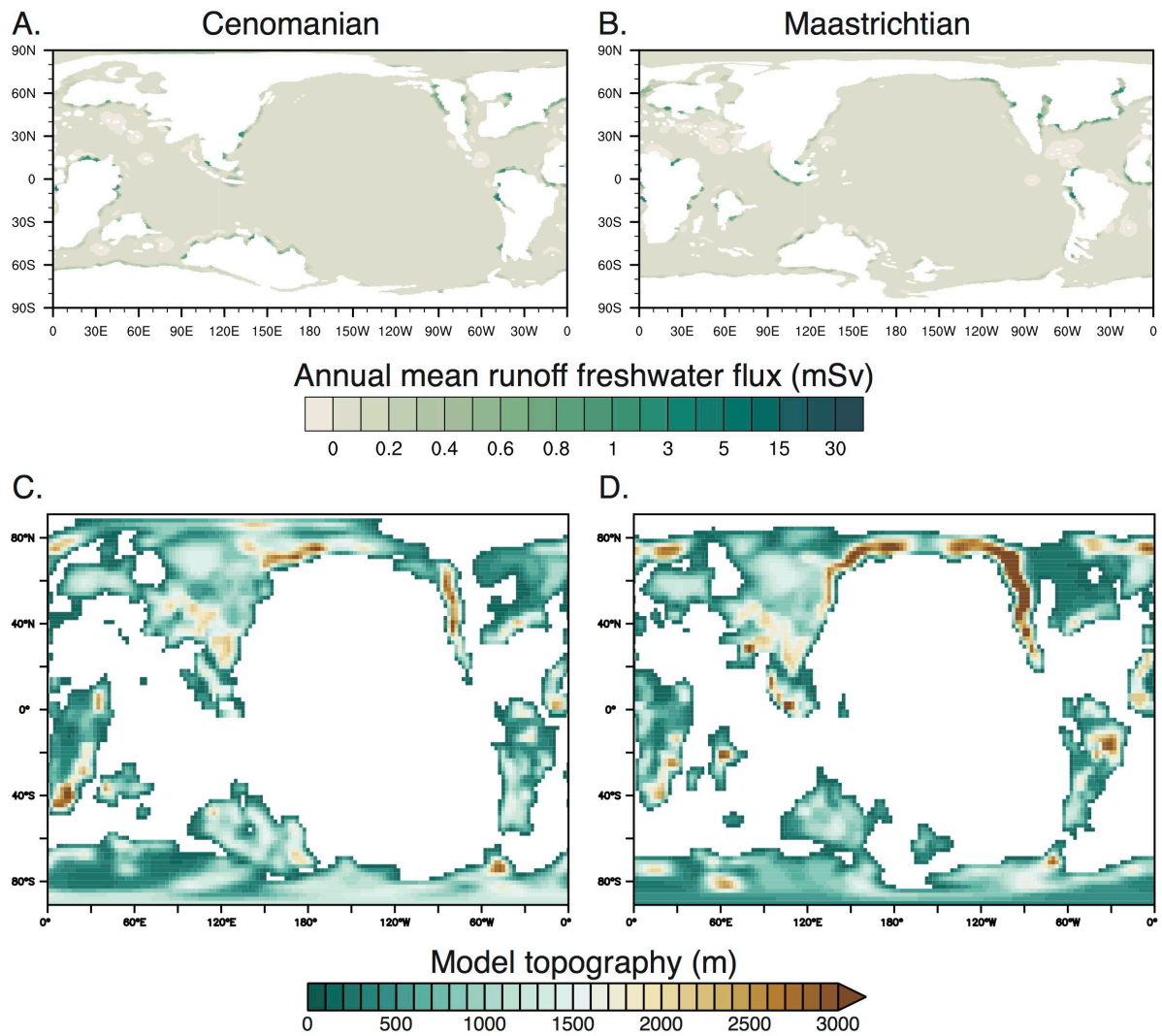


Figure S20. Annual mean runoff freshwater discharge into the ocean (mSv) for (A) the Cenomanian and (B) the Maastrichtian simulations. (C) Cenomanian topography seen by the CAM4 atmospheric model. (D) Same for the Maastrichtian.

58
 59
 60
 61
 62
 63
 64
 65

66 **References**

- 67 Doubrovine, P. V., and Tarduno, J. A.: Late Cretaceous paleolatitude of the Hawaiian hot
68 spot: New paleomagnetic data from Detroit Seamount (ODP Site 883), *Geochemistry,*
69 *Geophysics, Geosystems*, 5, 2004.
- 70 Frank, T. D., Thomas, D. J., Leckie, R. M., Arthur, M. A., Bown, P. R., Jones, K., and Lees, J.
71 A.: The Maastrichtian record from Shatsky Rise (northwest Pacific): A tropical
72 perspective on global ecological and oceanographic changes, *Paleoceanography*, 20,
73 2005.
- 74 Gradstein, F. M., and Ludden, J. N.: 43. Legs 122 and 123, northwestern Australian
75 margin—a stratigraphic and paleogeographic summary, *Proceedings of the Ocean*
76 *Drilling Program, Scientific Results*, 1992, 801-816,
- 77 Hague, A. M., Thomas, D. J., Huber, M., Korty, R., Woodard, S. C., and Jones, L. B.:
78 Convection of North Pacific deep water during the early Cenozoic, *Geology*, 40, 527-530,
79 10.1130/g32886.1, 2012.
- 80 Haynes, S. J., MacLeod, K. G., Ladant, J. B., Vande Guchte, A., Rostami, M. A., Poulsen, C. J.,
81 & Martin, E. E.: Constraining sources and relative flow rates of bottom waters in the Late
82 Cretaceous Pacific Ocean, *Geology*, 2020.
- 83 Jiménez Berrocoso, Á., MacLeod, K. G., Martin, E. E., Bourbon, E., Londoño, C. I., and
84 Basak, C.: Nutrient trap for Late Cretaceous organic-rich black shales in the tropical
85 North Atlantic, *Geology*, 38, 1111-1114, 2010.
- 86 Le Houedec, S., Meynadier, L., Cogné, J. P., Allègre, C. J., and Gourlan, A. T.: Oceanwide
87 imprint of large tectonic and oceanic events on seawater Nd isotope composition in the
88 Indian Ocean from 90 to 40 Ma, *Geochemistry, Geophysics, Geosystems*, 13, 2012.
- 89 MacLeod, K. G., Martin, E. E., and Blair, S. W.: Nd isotopic excursion across Cretaceous
90 ocean anoxic event 2 (Cenomanian-Turonian) in the tropical North Atlantic, *Geology*, 36,
91 811-814, 2008.
- 92 MacLeod, K. G., Londoño, C. I., Martin, E. E., Berrocoso, Á. J., and Basak, C.: Changes in
93 North Atlantic circulation at the end of the Cretaceous greenhouse interval, *Nature*
94 *Geoscience*, 4, 779, 2011.
- 95 Martin, E. E., MacLeod, K. G., Berrocoso, A. J., and Bourbon, E.: Water mass circulation on
96 Demerara Rise during the Late Cretaceous based on Nd isotopes, *Earth and Planetary*
97 *Science Letters*, 327, 111-120, 2012.
- 98 Masson, D. G., Montadert, L., and Scrutton, R. A.: Regional Geology of the Goban Spur
99 continental margin, *Initial Reports of the Deep Sea Drilling Project*, 80, 1115-1139, 1985.
- 100 Moiroud, M., Pucéat, E., Donnadiou, Y., Bayon, G., Guiraud, M., Voigt, S., Deconinck, J.-F.,
101 and Monna, F.: Evolution of neodymium isotopic signature of seawater during the Late
102 Cretaceous: Implications for intermediate and deep circulation, *Gondwana Research*, 36,
103 503-522, 2016.
- 104 Murphy, D. P., and Thomas, D. J.: Cretaceous deep-water formation in the Indian sector
105 of the Southern Ocean, *Paleoceanography*, 27, PA1211, 10.1029/2011pa002198, 2012.
- 106 Murphy, D. P., and Thomas, D. J.: The evolution of Late Cretaceous deep - ocean
107 circulation in the Atlantic basins: Neodymium isotope evidence from South Atlantic drill
108 sites for tectonic controls, *Geochemistry, Geophysics, Geosystems*, 14, 5323-5340, 2013.
- 109 Robinson, S. A., Murphy, D. P., Vance, D., and Thomas, D. J.: Formation of "Southern
110 Component Water" in the Late Cretaceous: Evidence from Nd-isotopes, *Geology*, 38, 871-
111 874, 10.1130/g31165.1, 2010.

112 Robinson, S. A., and Vance, D.: Widespread and synchronous change in deep-ocean
113 circulation in the North and South Atlantic during the Late Cretaceous,
114 *Paleoceanography*, 27, n/a-n/a, 10.1029/2011pa002240, 2012.
115 Thomas, D. J.: Evidence for deep-water production in the North Pacific Ocean during the
116 early Cenozoic warm interval, *Nature*, 430, 65, 2004.
117 Thomas, D. J., Korty, R., Huber, M., Schubert, J. A., and Haines, B.: Nd isotopic structure of
118 the Pacific Ocean 70–30 Ma and numerical evidence for vigorous ocean circulation and
119 ocean heat transport in a greenhouse world, *Paleoceanography*, 29, 454-469, 2014.
120 Voigt, S., Jung, C., Friedrich, O., Frank, M., Teschner, C., and Hoffmann, J.: Tectonically
121 restricted deep-ocean circulation at the end of the Cretaceous greenhouse, *Earth and
122 Planetary Science Letters*, 369, 169-177, 2013.
123